Title

Electrostatics and depletion determine competition between 2D nematic and 3D bundled phases of rod-like DNA nanotubes

Journal

Soft Matter, 12(23)

ISSN

1744-683X

Authors

Park, Chang-Young
Fygenson, Deborah K
Saleh, Omar A

Publication Date

2016-06-21

DOI

10.1039/c6sm00222f

Peer reviewed

Volume 12 | Number 23 | 21 June 2016 | Pages 5063–5234

Soft Matter

www.softmatter.org

ISSN 1744-683X

ROYAL SOCIETY OF CHEMISTRY

PAPER
Omar A. Saleh *et al.*
Electrostatics and depletion determine competition between 2D nematic and 3D bundled phases of rod-like DNA nanotubes

175 YEARS

Soft Matter

PAPER

View Article Online
View Journal | View Issue

Cite this: *Soft Matter*, 2016, 12, 5089

Electrostatics and depletion determine competition between 2D nematic and 3D bundled phases of rod-like DNA nanotubes†

Chang-Young Park,‡[a] Deborah K. Fygenson[b] and Omar A. Saleh*[c]

Received 27th January 2016,
Accepted 19th April 2016

DOI: 10.1039/c6sm00222f

www.rsc.org/softmatter

Rod-like particles form solutions of technological and biological importance. In particular, biofilaments such as actin and microtubules are known to form a variety of phases, both *in vivo* and *in vitro*, whose appearance can be controlled by depletion, confinement, and electrostatic interactions. Here, we utilize DNA nanotubes to undertake a comprehensive study of the effects of those interactions on two particular rod-like phases: a 2D nematic phase consisting of aligned rods pressed against a glass surface, and a 3D bundled network phase. We experimentally measure the stability of these two phases over a range of depletant concentrations and ionic strengths, finding that the 2D phase is slightly more stable than the 3D phase. We formulate a quantitative model of phase stability based on consideration of pairwise rod–rod and rod–surface interactions; notably, we include a careful accounting of solution electrostatics interactions using an effective-charge strategy. The model is relatively simple and contains no free parameters, yet predicts phase boundaries in good agreement with the experiment. Our results indicate that electrostatic interactions, rather than depletion, are largely responsible for the enhanced stability of the 2D phase. This work provides insight into the polymorphism of rod-like solutions, indicating why certain phases appear, and providing a means (and a predictive model) for controlling those phases.

1 Introduction

Solutions of rigid, rod-like macromolecular filaments display a variety of structural transitions that derive from the large aspect ratio of such particles, and the interplay of that aspect ratio with various solution-mediated interactions. Control and understanding of the various structures has technological relevance, particularly as rod-like particles can affect rheological properties of solutions at much lower volume fractions than spherical particles.[1] Significant interest in the polymorphism of solutions of rods is derived from biology: rod-like biofilaments, such as actin, microtubules, and intermediate filaments, define the structure and mechanics of the cell and its organelles. Prior work has investigated the physics of *in vitro* solutions of filamentous biopolymers. Some work has been done on microtubule solutions.[2–5] A more extensive body of work has explored various aspects of actin solutions, including experimental studies of their structure[6–10] and rheology,[11–13] along with theoretical studies of the influence of inter-particle interactions on phase behavior.[14–17]

In biological situations, actin and microtubules are subject to two physical effects that strongly influence their structure: crowding, or depletion, interactions caused by the large volume fraction of soluble protein in the cytoplasm, and confinement by the cell membrane. Depletion leads to attractive interactions that bind and align filaments since solute translational entropy is maximized by bringing the filaments together, according to the Asakura–Oosawa description.[18] These attractions are balanced by repulsions that are frequently electrostatic due to the highly-charged nature of the biopolymers. In certain conditions of weakened electrostatics and/or high depletant concentrations, the balance of attractive and repulsive forces results in bound states that, *in vitro*, lead to bundling and network (hydrogel) formation by the filaments.

Depletion leads to attractive interactions between filaments and confining surfaces, as excluded volume is also minimized by adsorption of the rods onto a flat interface, leading to two-dimensional (2D), or near-2D, structures that can display nematic liquid-crystalline order.[8,9,19] It has been suggested that biologically-observed membrane-proximal ('cortical') organized 2D arrays of actin could be favored by the combination of confinement and depletion.[8] Organized cortical 2D arrays occur

[a] *Material Research Laboratory, University of California, Santa Barbara, CA 93106, USA*
[b] *Department of Physics and Biomolecular Science and Engineering Program, University of California, Santa Barbara, CA 93106, USA*
[c] *Materials Department and Biomolecular Science and Engineering Program, University of California, Santa Barbara, CA 93106, USA. E-mail: saleh@engr.ucsb.edu*

† Electronic supplementary information (ESI) available. See DOI: 10.1039/c6sm00222f

‡ Current address: Seoul, South Korea.

with microtubules in plant cells,[20,21] and are also plausibly explained as being favored by confinement and depletion. Finally, these mechanisms have been exploited in recent experimental studies of active matter systems, in which depletion and surface confinement are used to create striking and easily-imaged aligned phases of actin[9] or microtubules[19] that restructure due to the driving forces of embedded motor proteins.

Despite the extensive biologically-motivated interest in surface-confined, crowded solutions of rod-like polymers, there has not been a systematic study of the structure and relative stability of 3D phases *versus* 2D phases. Here we perform such a study by carefully modulating the attractive and repulsive interactions among rod-like filaments, and between rods and a surface, then imaging the resultant 2D and 3D phases using fluorescence microscopy. As a model system, we use rods self-assembled from DNA strands through sequence-specific basepairing, *i.e.* so-called 'DNA nanotubes' (NTs). These NTs, developed and characterized previously,[22] are easily fluorescently labeled, robust, and highly-soluble; thus, NTs present an ideal experimental system in which to explore the physics of rod solutions. The NTs we use have persistence lengths of about 20 μm,[23] making them mechanically nearly identical to actin. The use of DNA imparts onto the NTs a very high charge density, which in turn permits control of repulsive electrostatic interactions by varying the amount of added salt in the solution. Attractive interactions are controlled through the use of a depletant, particularly by adding small amounts of the neutral polymer methylcellulose (MC) to the solution.

Our experimental results, using DNA NTs and a glass confining surface, show a slightly increased stability of a nematic 2D phase over a bundled 3D network phase, which we attribute to the increased excluded-volume interaction of a rod with a flat surface relative to that with another rod, along with the relatively low charge density of the glass surface. We quantify this contention through a calculation of the phase boundary for both 2D and 3D phases, as estimated by considering the pairwise depletion and electrostatic interactions that lead to the stable bound states underlying each structure. Compared to prior work,[7,16] our model is simple to implement, and handles electrostatic interactions between rods in a carefully-justified fashion. Further, our model uses no free parameters, yet achieves excellent agreement with the measured phase regions. We suggest that this simple model could be useful in the application to other systems of rod-like polymers.

2 Methods

NTs are assembled from six phosphorylated, single-stranded DNA oligos (Integrated DNA Technologies), with lengths ranging from 17 nt to 42 nt. Their sequences are based on the oligos named SE1, SE2, SE3, SE4, SE5, and SE6-2 in ref. 24; see ESI† for details. For visualization, 20% of the SE3 oligos are labeled with a fluorescent dye (Cy3) on the 5′-end. NTs are made by mixing the six oligos, each at a concentration of 6 μM, in a buffer suitable for ligation (T4 DNA ligase buffer, New England Biolabs). The solution is heated to 95 °C, then allowed to slowly cool. The tubes are then ligated by adding T4 ligase, ATP and DTT (New England Biolabs) in the recommended conditions and incubating overnight. Ligation components and excess oligos are then removed using an Amicon Ultra centrifugal filter (30 kDa cutoff), and the ligated NTs are resuspended in the desired Tris-HCl buffer concentration (pH 7.5).

The NT solution is then mixed with methylcellulose (MC; Sigma Aldrich, M7140; approximate M.W. 14 000); both the MC and the buffer concentrations are varied as specified. The final solution concentration of tiles (equivalent to the concentration of each oligo) is 2 μM. The solution is mixed in a microcentrifuge tube and transferred to a clean glass capillary tube, which is then sealed. The capillary tubes are annealed at 45 °C over 4 hours, then slowly cooled down to room temperature.

DNA NT assembly is a hierarchical process, in which the six oligos form tiles, and tiles then assemble both laterally to form the tube circumference, and longitudinally to form the tube length.[22] The resulting NT is a ∼10 nm diameter tube formed from a cylindrical array of an estimated 14 double-helical DNAs stabilized by crossover junctions. The average length of the NTs, using the assembly process described above, is roughly 5 μm, with a range from 0.5 μm to 50 μm. Finally, the ligated NTs are extremely stable over time: we have observed NTs to retain their form for over a month, matching prior observations of the stability of ligated NTs.[23]

The final structure of the NT solutions are measured with two fluorescent microscopes: lower magnification structure measurement is performed with an epi-fluorescent microscope (IX71, Olympus) using a 10× or 20× objective, both with and without a polarizer in the emission pathway. Higher-resolution structural images are obtained with a laser-scanning confocal microscope (Fluoview 1200, Olympus).

3 Experimental results

3.1 2D nematic phase

At moderate concentrations of depletant and buffer, we find that the DNA NTs form a striking, quasi-two-dimensional nematic liquid crystal next to the glass surface. Typical images of this structure, using 0.35 wt% MC and 10 mM Tris HCl, are shown in Fig. 1. Low magnification epi-fluorescence images show textured domains we interpret as being formed by patches of aligned NTs, with different patches having different orientations. This is confirmed in two ways: first, it is known that certain fluorophores attached to DNA oligos within NTs tend to emit light polarized perpendicular to the NT axis, apparently due to orientation of the fluorophore by the NT structure.[25] Thus, by placing a polarizer in the emission pathway, we can immediately visualize the varying NT orientation through the varying fluorescence intensity – indeed, such images (Fig. 1c) display intensity variations that match the texture variation seen without the polarizer, and are consistent with patches of a few tens of microns in size.

As an alternate confirmation, we visualize the film at high resolution in a laser-scanning confocal microscope. In this instrument,

Fig. 1 (a) Sketch of the experimental arrangement. (b and c) Aligned DNA nanotubes near a glass surface visualized with a fluorescence microscope both without (b) and with (c) a horizontally-oriented polarizer. (d) Laser-scanning confocal image of aligned DNA nanotubes. Image dimensions are (b and c) (320 μm)^2 (d) (150 μm)^2.

individual NTs can be resolved, and the images again confirm the formation of a nematic structure with 10–100 μm patch sizes. Further, using the confocal, we can take a series of images normal to the glass surface (a z-stack), which indicates that the thickness of the 2D layer is approximately 1 μm, with some NT bundles forming above the layer (seen as bright lines in Fig. 1d). Note that, due to polarization of the excitation beam in the confocal instrument, patches of varying orientation have varying brightness, giving Fig. 1d a contoured appearance.

3.2 Polymorphic structure

To probe the robustness of the 2D nematic phase over varying solution conditions, we prepare a series of NT solutions with different MC concentrations (from 0.1 wt% to 0.9 wt%) and different Tris-HCl concentrations (from 1 to 30 mM). These variations are expected to alter phase stability, since the amount of MC will alter the depletion attraction, while the amount of Tris-HCl alters the solution ionic strength, which affects electrostatic interactions through screening. Capillaries are prepared containing NTs, and the various amounts of MC and buffer, annealed, sealed, and allowed to equilibrate for several days before imaging. Each capillary is then imaged using both low-resolution epi-fluorescent microscopy (to resolve structures in the bulk solution in the center of the capillary), and laser-scanning confocal microscopy (to test for the presence of the nematic layer on the capillary surface). A series of images of varying MC concentration, and constant [Tris-HCl] = 10 mM, is shown in Fig. 2; a complementary series of images, of varying Tris-HCl concentration and constant 0.4 wt% MC, is shown in Fig. 3. In the latter figure, images next to the glass surface are omitted when no structure is seen.

At low concentrations of depletant and/or at low ionic strength, no structure is observed; instead, the images in those regimes display a roughly uniform fluorescence indicative of an isotropic solution of NTs. As MC concentration or ionic strength is increased, we observe the emergence of, first,

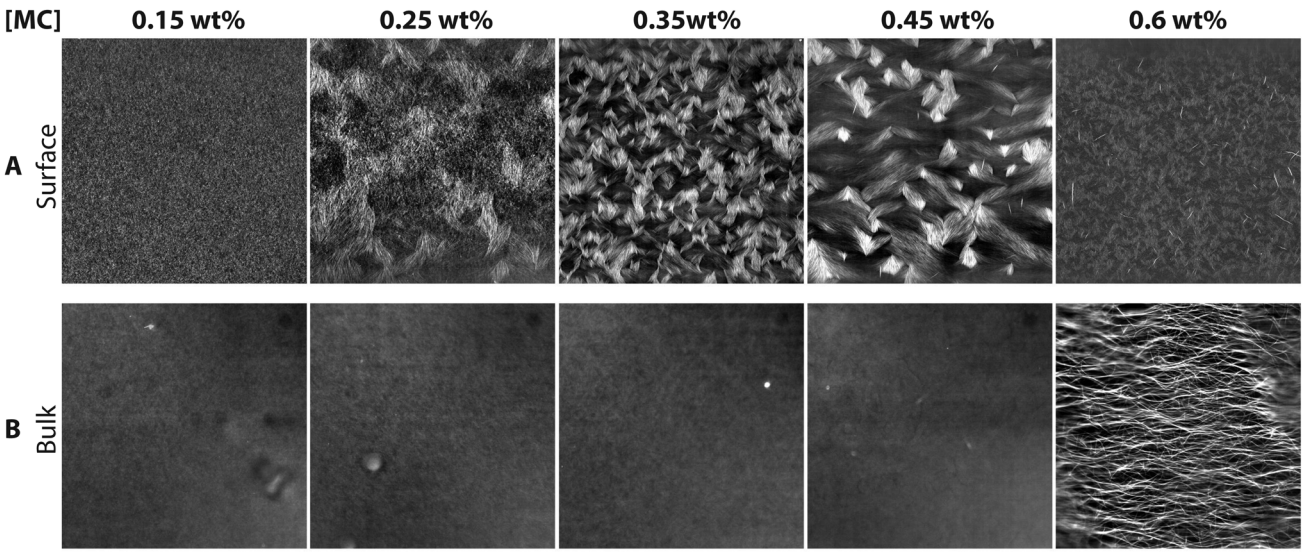

Fig. 2 DNA NT phases in varying amounts of methylcellulose (MC) at constant buffer concentration, [Tris-HCl] = 10 mM. (A) Laser-scanning confocal images of NTs near the glass surface. (B) Conventional epi-fluorescent images of the solution away from the glass surface. By increasing the concentration of MC, DNA NTs first form a nematic phase near the glass surface, then form bundles in the bulk. Image dimensions are (A) (635 μm)^2 and (B) (640 μm)^2.

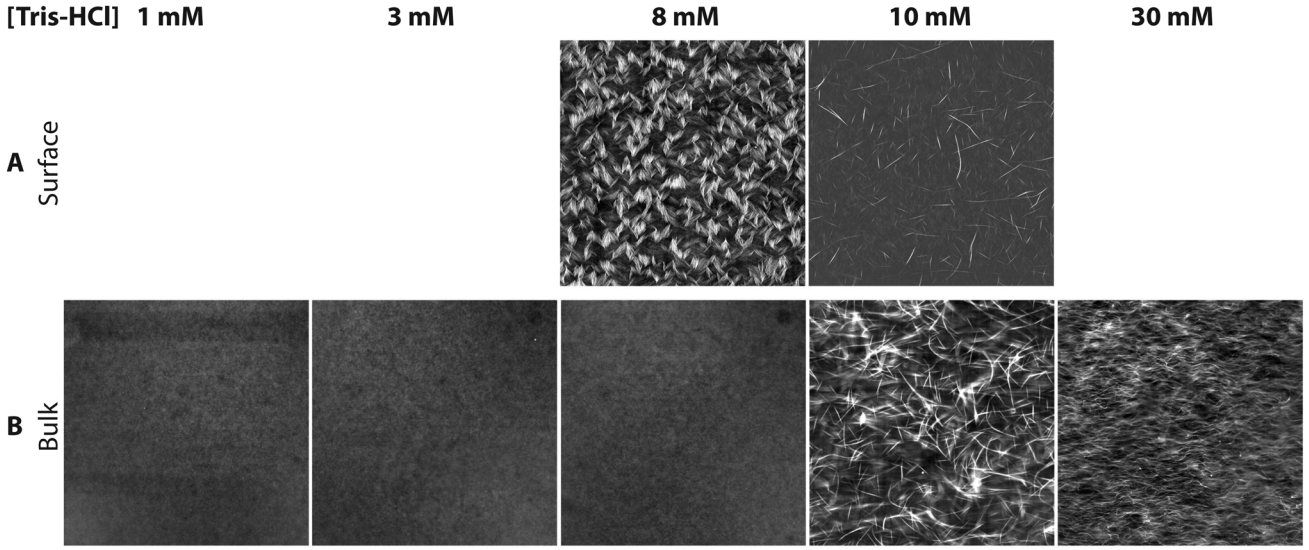

Fig. 3 DNA NT phases in varying concentration of buffer, Tris-HCl, at constant [MC] = 0.4 wt%. (A) Laser-scanning confocal images of NTs near the glass surface; conditions lacking significant structure near the surface are not shown. (B) Conventional epi-fluorescent images of the solution away from the glass surface. By increasing the concentration of buffer, DNA NTs first form a nematic phase near the glass surface, then form bundles in the bulk. Image dimensions are (A) (635 μm)^2 and (B) (640 μm)^2.

the 2D nematic layer, then a 3D phase consisting of a network of bundled NTs. These observations are consistent with expectations: increasing MC will increase the depletion attraction, stabilizing bound states of NTs with NTs, or NTs with the glass surface. Increasing the ionic strength will screen electrostatic effects, decreasing the mutual repulsion between the highly charged NTs, as well as the repulsion between the NTs and the like-charged glass surface, enabling stable bound states to form at lower MC concentrations.

Our experimental results indicate a likely role being played by kinetic effects: we observe that the appearance of the 2D phase is greatly diminished when the 3D structured phase appears. This occurs despite, as detailed below, the expectation that the 2D phase should be energetically favored over the 3D phase. We interpret this as a kinetic trapping phenomena: in conditions where NT–NT interactions are strongly attractive, the NTs will bundle immediately upon forming the mixture (*i.e.* within the microcentrifuge tube, before transfer to the capillary). Formation of the 2D phase in the capillary would then require dissolution of a bundle and transfer of the NTs to the surface, a process which is energetically unfavorable in those conditions. In essence, we posit that the 3D bundled network is a robust metastable phase favored by the particular experimental process we used, and whose appearance greatly slows the formation of the equilibrium 2D nematic layer.

Our experimental results are summarized in Fig. 4A, which shows a phase diagram of the appearance of the unstructured (isotropic) solution, the aligned 2D nematic film, and the 3D bulk bundles.

3.3 Modeling of the phase diagram through quantification of pairwise tube interactions

The experimental results establish that electrostatic interactions and depletion interactions can be separately tuned to control the appearance of the 2D (film) and 3D (bundled network) phases of the DNA NT system. A notable finding is that the 2D phase appears at lower depletant concentrations and lower salt concentrations than the 3D phase – that is, the 2D phase is more stable under conditions of larger net repulsive interactions. Similar results were found for actin solutions.[8] Here, we use analytical theory, in which we model the NTs as rods with a fixed size and surface charge, to show that this behavior is consistent with the larger attractive depletion interaction, and weaker electrostatic interaction, of the rod/surface pair compared with the rod/rod pair. We formulate a simple model based on pairwise interactions that roughly predicts the observed phase diagram, with no free parameters (Fig. 4)

Our model is based on the assumption that the appearance of a stable 2D or 3D phase will be correlated with the appearance of a stable bound state in the energy/distance curve describing the pairwise rod/surface or rod/rod interaction. Such a pairwise model ignores many-body effects that can be important to phase stability; indeed, prior theories are more complete in that respect.[16] However, at the core of those models are pairwise interactions; as such, we expect our approach to provide approximately correct guidelines for phase stability.

We quantify the pairwise interaction energy $u_{rr}(d)$ between parallel rods, and the interaction $u_{rs}(d)$ between a rod parallel to a surface, as a function of d, the surface to surface separation (*i.e.* gap extent) between the interacting partners. In both cases, the interaction energy is found as the sum of a depletion term, $w(d)$, and an electrostatic term, $v(d)$: $u_{rr/rs}(d) = w_{rr/rs}(d) + v_{rr/rs}(d)$. We calculate all energies on a per-filament basis so as to facilitate comparison between the rod/surface interaction (which has a bound state with only a single filament), and the rod/rod interaction (which has a bound state with two filaments). We assume relatively long rods (consistent with the experimental

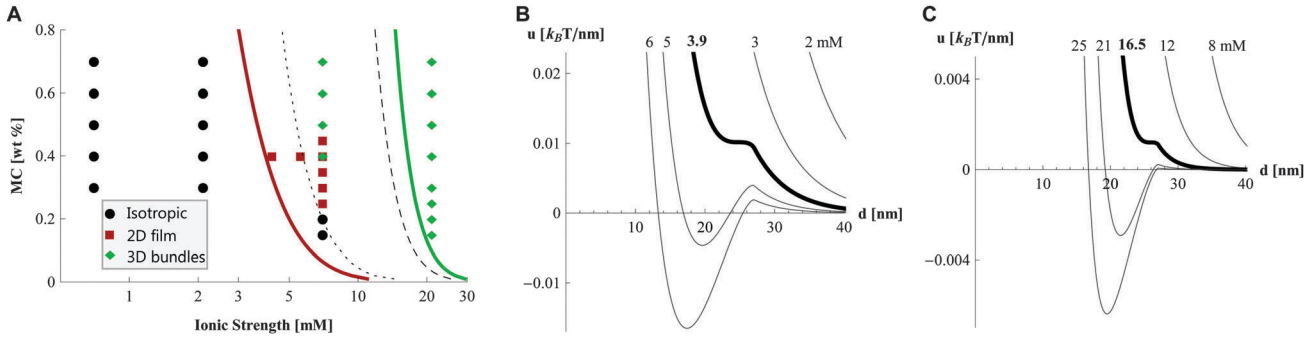

Fig. 4 (A) Phase diagram of the DNA NT system, as modulated by ionic strength and depletant (MC) concentration. Experimental observations are shown as points. The thick red (green) line indicates the calculated phase boundary for the 2D (3D) phase, using the pairwise model described in the text. The black lines indicate the phase boundaries calculated by mixing the rod/rod and rod/surface interactions, for the purpose of determining the relative importance of electrostatic and depletion interactions: the dashed line utilizes rod/rod electrostatics with rod/surface excluded volume, while the dotted line utilizes rod/surface electrostatics with rod/rod excluded volume. (B and C) Interaction energies $u(d)$ *vs.* separation distance d for (B) the rod/surface interaction, and (C) the rod/rod interaction, at [MC] = 0.4 wt% and for a variety of ionic strengths (labeled) in the vicinity of each phase boundary. Bold lines/labels indicate $u(d)$ on each phase boundary.

ratios of length to diameter that are ≥ 50), and consequently neglect end effects. Further, we report all energies per unit length, and in units of the thermal energy k_BT.

3.3.1 The depletion interaction. The depletion energy per unit length, in k_BT units, is $w(d) \approx \Pi A_{ov}(d)/k_BT$, where Π is the osmotic pressure of depletants, and A_{ov} is the overlap area per filament between the interacting partners. At the relatively small depletant concentrations c used in this study, the osmotic pressure can be estimated as $\Pi \approx ck_BT$. The overlap volume, which is $A_{ov}L$ for rods of length L, corresponds to the volume inaccessible to the depletant when the system is at separation d, compared to that accessible at large separations. We calculate A_{ov} by treating the depletant (MC) as hard particles of radius $\rho = 2R_g/\sqrt{\pi}$, where $R_g \approx 13$ nm is the radius of gyration of the average chain. The factor of $2/\sqrt{\pi}$ matches the extent R_g of the polymer chain to the radius of a hard sphere with an equivalent depletion effect.[26] A_{ov} is zero for $d > 2\rho$, since depletants can enter such large gaps. For $d < 2\rho$, the overlap area per filament has a similar form for both geometries: $A_{ov,rr/rs}(d) = (r+\rho)^2\left(\arccos \alpha_{rr/rs} - \alpha_{rr/rs}\sqrt{1-\alpha_{rr/rs}{}^2}\right)$, where r is the rod radius. The constant α differs for the two geometries: for the rod/surface interaction, $\alpha_{rs} = (d + r - \rho)/(r + \rho)$, while for the rod/rod interaction, $\alpha_{rr} = (d/2 + r)/(r + \rho)$.

3.3.2 The electrostatic interaction. To model the electrostatic interaction, we must account for the concentration-dependent screening effect of the salt solution. We achieve this using the Debye–Huckel (DH) approximation of the Poisson–Boltzmann solution electrostatic theory. Poisson–Boltzmann is justified for the monovalent salt solutions used in the experiment, since such ions are weakly-interacting, and so satisfy the mean-field assumptions of the theory.

The use of the DH approximation is justified based on careful consideration and handling of the charge density of the DNA nanotubes and the glass surface. DH is a linear approximation to the otherwise non-linear Poisson–Boltzmann (NLPB) theory. DH holds only in the limit of low potentials, and thus low charge density of the macroscopic object.[27] For planar surfaces, the DH limit is validated if the Gouy–Chapman length, $b \equiv 1/(2\pi\sigma l_B)$, is much larger than the solution Debye length, $\lambda_D(n_0) \equiv \sqrt{8\pi l_B n_0}$, where σ is the surface number density of charges on the plane, $l_B \approx 0.714$ nm is the Bjerrum length, and n_0 is the ionic strength of the solution[27]. For clean glass surfaces, the charge density is about 0.002 nm^{-2},[28] so $b \approx 111$ nm. For the buffer concentrations used here ([Tris-HCl] = 1–30 mM), the ionic strengths range from 0.7 to 21 mM, giving Debye lengths of 11.5 to 2.1 nm. Therefore, regarding the glass surface, the experiments are always conducted in the limit $b/\lambda_D \gg 1$, and DH is a good approximation.

3.3.2.1 Electrostatics of DNA NTs: the effective-charge Debye–Huckel model. Unlike the glass surface, the NTs are extremely highly charged: the tubes have a radius of $r \approx 5$ nm, and are effectively comprised of roughly 14 double-stranded DNA molecules, each of which carry 2 bare charges per basepair. The surface charge of the rods are thus $\sigma_{rod} \approx 2.6$ nm^{-2}, which leads to a Gouy–Chapman length $b_{rod} \approx 0.1$ nm. This would seem to necessitate the use of NLPB to calculate the potential of the rods. However, a body of work has established that, at distances $d \gg \lambda_D$, the potential calculated from NLPB for a highly-charged, finite-diameter rod matches that calculated for a line charge from DH, so long as the correct effective line charge density, ν_{eff}, is used in the DH calculation.[29–32] Numerical solutions of NLPB for the potential around a rod provide quantitative estimates of ν_{eff} as a function of rod diameter, charge, and solution salt concentration.[29,32] This 'effective-charge DH' approach has been used previously for both charged rods in liquid crystals,[30] and for interacting DNA molecules.[31,32]

To apply this approach, it must be established that the modeled situation is in the far-field limit ($d \gg \lambda_D$). While in some regions of the phase diagram there are likely to be bound states whose separation is not much larger than λ_D, we nonetheless justify the use of the effective-charge DH approach with the following argument: our aim is to calculate the phase boundary for a pairwise interaction. The phase boundary corresponds to the initial appearance of a bound state in $u(d)$. Since this bound

state is stabilized by the attractive depletion interaction, it will first appear at separations slightly less than the depletant diameter, $d \lesssim 2\rho \approx 26$ nm. Since $2\rho \gg \lambda_D$ for all but the lowest salt concentration, the relevant interactions will indeed be in the far-field limit in the vicinity of the phase boundary, justifying the use of DH with an effective charge ν_{eff} for the rods. The lack of applicability at low salt is not a serious impediment, as both the experimental and calculated phase boundaries occur at higher salt.

To apply the effective-charge DH model, we first calculate ν_{eff} using the approach described by Neukirch and Marko,[32] which itself relies upon the numerical work of Stigter.[29] In particular, we set

$$\nu_{eff} = \frac{\nu\lambda_D}{\gamma r K_1(r/\lambda_D)} \quad (1)$$

where K_n is the nth modified Bessel function of the second kind, $\nu \approx 84$ nm^{-1} is the bare line charge density of the rod, and $\gamma = \gamma(r, \nu, \lambda_D)$ is a numerical correction factor found from Stigter's work[29] (see ESI† for details). Given the bare charge density of 84 nm^{-1}, and for the experimental ionic strengths of 0.7, 2.1, 5.6, 7, and 21 mM, we find effective charges of, respectively, ν_{eff} = 56, 65, 87, 95, and 211 nm^{-1}.

The electrostatic energy for each geometry is then found by placing a rod of charge ν_{eff} into the DH potential calculated for the glass surface, or a second rod. In particular, the rod/surface electrostatic interaction energy is

$$v_{rs}(d) = 2\nu_{eff}\frac{\lambda_D}{b}e^{-(d+r)/\lambda_D}, \quad (2)$$

and the rod–rod energy is:

$$v_{rr}(d) = \nu_{eff}{}^2 l_B K_0[(d + 2r)/\lambda_D]. \quad (3)$$

3.3.2.2 Estimating phase boundaries from pairwise interactions. Given the set of depletion and electrostatic interactions w_{rs}, w_{rr}, v_{rs} and v_{rr}, we calculate the total interaction $u_{rr/rs}(d)$, and use it to estimate the position of the phase boundary at which the bound state emerges. In particular, we define a given salt/depletant condition to be on the phase boundary if there exists, in that condition, a single separation, d_c, for which $u'(d_c) = 0$ and $u''(d_c) = 0$ (see Fig. 4B and C). The phase boundaries thus calculated, for both rod/rod and rod/surface interactions, are in relatively good agreement with the experimental data, as shown in Fig. 4A: as observed experimentally, the calculated rod/surface bound state is stable at a slightly lower range of salt, with both experimental and theoretical transitions occurring at $\approx$4 mM ionic strength for the rod/surface state, and $\approx$16 mM ionic strength for the rod/rod state, at 0.4 wt% MC.

The model does underestimate the stability of the 3D bundled-network phase – note particularly the occurrence of stable bundles at 10 mM ionic strength and high depletant concentrations. This could be due to limitations in the approximations in the electrostatic model discussed above. Or, it could be due to degrees of freedom in the rod–rod-interaction that are not modeled in our simple theory – notably, formation of bundles of many rods could provide, through many-body effects, extra stability compared to that found from our simple pairwise model. Such many-body effects have been postulated to play a role in rod-bundling in the context of attractions induced by counterion fluctuations.[33] Alternatively, relative rotations (twists or splays) between neighboring rods could decrease electrostatic repulsions – indeed, prior work has shown that charged rods prefer mutually-perpendicular cubatic phases in certain conditions.[16]

The phase boundaries in Fig. 4A are relatively vertical over the experimentally-tested region, indicating an insensitivity to depletant concentration that, in turn, argues that electrostatic differences are the dominant reason for the differing rod/rod and rod/surface phase boundaries. To test that hypothesis, we calculate the phase boundaries from the pairwise model with interactions that are mixed between the rod/rod and rod/surface cases. That is, we calculated the phase boundaries for a model where the pair potential is given by $w_{rs}(d) + v_{rr}(d)$ (using rod/surface for depletion, and rod/rod for electrostatics; this is shown in the dashed line in Fig. 4A), and also for a pair potential $w_{rr}(d) + v_{rs}(d)$ (using rod/rod for depletion, and rod/surface for electrostatics; this is shown in the dotted line in Fig. 4A). The dashed line is quite close to the (unmixed) rod/rod phase boundary, while the dotted line is close to the rod/surface boundary, indicating that swapping the depletion interactions does not strongly affect the phase behavior. In marked contrast, the dashed line is quite far from the rod/surface boundary, and the dotted line is far from the rod/rod boundary, indicating that swapping the electrostatic interactions has a very strong effect on phase stability.

The dominance of electrostatics in our system can be attributed to the huge charge on the DNA NTs that disfavors rod/rod pairing. This indicates that the stability of the 2D state can be optimized either by increasing the rod charge, or decreasing the surface charge – so 2D nematics can be made more stable using relatively neutralized surfaces. While depletion effects indeed favor the 2D nematic over the 3D bundled phase, this effect is minimal, and charge density modulation is a better experimental strategy for stabilizing the 2D film.

4 Conclusion

We have performed a systematic study of the interplay of depletion attractions and electrostatic repulsions in stabilizing 2D nematic films, and 3D bundled networks, of DNA NTs. Our experimental work demonstrates that DNA NTs are an effective and useful model of the phase behavior of rod-like solutions, particularly as the NTs replicate the phases seen in prior work with actin.[8] The NTs offer several experimental features that facilitate their use as a model system, including the fluorophore orientation effect that permits facile measurement of NT alignment using polarized fluorescence microscopy. A further advantage, which we did not exploit here, is reconfigurability: unlike actin or microtubules, DNA NTs can be programmed to have a variety of diameters and charge densities.[22] Future investigations could exploit this ability to further test and refine models of rod interactions.

Our experimental results demonstrate an increased stability of the 2D phase over the 3D phase. We attribute this to a combination of the larger depletion attraction of a rod with a flat surface *versus* that with a second rod, and the relatively low charge density of the glass surface. We validate these ideas using a quantitative model of the pairwise depletion and electrostatic interactions among rods, and between rods and the surface. Our model is simple and lacks free parameters, yet it reproduces the measured phase diagram with relatively high fidelity. Further, by analysis of our model, we are led to conclude that the stability of the 2D phase is mainly due to the lower charge of the glass surface, and only slightly favored by the larger rod/surface depletion interaction. We expect our experimentally-validated pairwise model will have predictive utility particularly due to its relative simplicity, and could be utilized by researchers seeking to stabilize 2D phases in other systems.

Acknowledgements

The experimental studies in this work were supported by the Institute for Collaborative Biotechnologies through grant no. W911NF-09-0001 from the U.S. Army Research Office. The content of the information does not necessarily reflect the position or the policy of the Government, and no official endorsement should be inferred. Theoretical studies were supported by the U.S. Department of Energy (DOE), Office of Science, Basic Energy Sciences (BES), under Award # DE-SC0014427.

References

1 G. M. H. Wilkins, P. T. Spicer and M. J. Solomon, *Langmuir*, 2009, **25**, 8951–8959.
2 A. L. Hitt, A. R. Cross and R. C. Williams, *J. Biol. Chem.*, 1990, **265**, 1639–1647.
3 D. J. Needleman, M. A. Ojeda-Lopez, U. Raviv, K. Ewert, J. B. Jones, H. P. Miller, L. Wilson and C. R. Safinya, *Phys. Rev. Lett.*, 2004, **93**, 198104.
4 Y.-C. Lin, G. H. Koenderink, F. C. MacKintosh and D. A. Weitz, *Macromolecules*, 2007, **40**, 7714–7720.
5 Y. Yang, J. Lin, B. Kaytanli, O. A. Saleh and M. T. Valentine, *Soft Matter*, 2012, **8**, 1776–1784.
6 J. Goverman, L. A. Schick and J. Newman, *Biophys. J.*, 1996, **71**, 1485–1492.
7 M. Hosek and J. X. Tang, *Phys. Rev. E: Stat., Nonlinear, Soft Matter Phys.*, 2004, **69**, 051907.
8 D. Popp, A. Yamamoto, M. Iwasa and Y. Maéda, *Biochem. Biophys. Res. Commun.*, 2006, **351**, 348–353.
9 M. P. Murrell and M. L. Gardel, *Proc. Natl. Acad. Sci. U. S. A.*, 2012, **109**, 20820–20825.
10 F. Huber, D. Strehle, J. Schnauß and J. Käs, *New J. Phys.*, 2015, **17**, 043029.
11 M. L. Gardel, M. T. Valentine, J. C. Crocker, A. R. Bausch and D. A. Weitz, *Phys. Rev. Lett.*, 2003, **91**, 158302.
12 R. Tharmann, M. M. A. E. Claessens and A. R. Bausch, *Biophys. J.*, 2006, **90**, 2622–2627.
13 S. Köhler, O. Lieleg and A. R. Bausch, *PLoS One*, 2008, **3**, e2736.
14 I. Borukhov and R. F. Bruinsma, *Phys. Rev. Lett.*, 2001, **87**, 158101.
15 A. G. Zilman and S. A. Safran, *Europhys. Lett.*, 2003, **63**, 139–145.
16 I. Borukhov, R. F. Bruinsma, W. M. Gelbart and A. J. Liu, *Proc. Natl. Acad. Sci. U. S. A.*, 2005, **102**, 3673–3678.
17 R. J. Pandolfi, L. Edwards, D. Johnston, P. Becich and L. S. Hirst, *Phys. Rev. E: Stat., Nonlinear, Soft Matter Phys.*, 2014, **89**, 062602.
18 S. Asakura and F. Oosawa, *Chem. Phys.*, 1954, 1255–1256.
19 T. Sanchez, D. T. N. Chen, S. J. DeCamp, M. Heymann and Z. Dogic, *Nature*, 2012, **491**, 431–434.
20 A. Paradez, A. Wright and D. W. Ehrhardt, *Curr. Opin. Plant Biol.*, 2006, **9**, 571–578.
21 G. O. Wasteneys and J. C. Ambrose, *Trends Cell Biol.*, 2009, **19**, 62–71.
22 P. W. K. Rothemund, A. Ekani-Nkodo, N. Papadakis, A. Kumar, D. K. Fygenson and E. Winfree, *J. Am. Chem. Soc.*, 2004, **126**, 16344–16352.
23 P. O'Neill, P. W. K. Rothemund, A. Kumar and D. K. Fygenson, *Nano Lett.*, 2006, **6**, 1379–1383.
24 O. J. N. Bertrand, D. K. Fygenson and O. A. Saleh, *Proc. Natl. Acad. Sci. U. S. A.*, 2012, **109**, 17342–17347.
25 D. Schiffels, PhD thesis, Ludwig-Maximilians-Universität München, 2013.
26 H. N. Lekkerkerker and R. Tuinier, *Colloids and the depletion interaction*, Springer, 2011, vol. 833.
27 D. Andelman, *Proceedings of the Nato ASI & SUSSP on "Soft condensed matter physics in molecular and cell biology"*, 2006, pp. 97–122.
28 S. H. Behrens and D. G. Grier, *J. Chem. Phys.*, 2001, **115**, 6716–6721.
29 D. Stigter, *J. Colloid Interface Sci.*, 1975, **53**, 296–306.
30 A. Stroobants, H. Lekkerkerker and T. Odijk, *Macromolecules*, 1986, **19**, 2232–2238.
31 J. Ubbink and T. Odijk, *Biophys. J.*, 1999, **76**, 2502–2519.
32 S. Neukirch and J. F. Marko, *Phys. Rev. Lett.*, 2011, **106**, 138104.
33 B. Y. Ha and A. J. Liu, *Phys. Rev. Lett.*, 1998, **81**, 1011–1014.